In-Vehicle Human Detection and Seat Positioning via Respiration-Based IR-UWB Radar Sensing

Eunji Lee, Jihye Kim, Seong-Cheol Kim

Department of Electrical and Computer Engineering

Seoul National University

Seoul, Republic of Korea

{ej9309, jihyekim224, sckim}@maxwell.snu.ac.kr

Abstract—This paper proposes an algorithm for detecting humans and estimating their seat positions inside a vehicle using impulse radio ultra-wideband (IR-UWB) radar. The algorithm associates signals received from multiple radar sensors by matching identical respiration rates, thereby enabling accurate identification and localization of individuals. To optimize system performance, seven radar units were deployed at different locations, and the algorithm's effectiveness was evaluated across various sensor combinations. The proposed method achieved a human detection accuracy exceeding 99%. Furthermore, optimal radar configurations were identified, yielding over 70% seat positioning accuracy in scenarios involving large objects and up to two individuals, and over 98% accuracy in single-individual scenarios.

Index Terms—IR-UWB radar, respiration rate, human detection, seat positioning

I. INTRODUCTION

Recently, in-cabin monitoring systems have attracted significant attention for enhancing the safety and convenience of both drivers and passengers [1]. Among various functionalities, seat occupancy monitoring is a primary task, traditionally implemented using pressure sensors or cameras [2]. However, pressure sensors are prone to false alarms caused by non-human objects, while camera-based systems are sensitive to lighting conditions and raise concerns over privacy. In this context, radar has emerged as a promising alternative for seat occupancy monitoring, offering robustness against environmental variations and mitigating the aforementioned limitations [3], [4].

There are various types of radars classified by their waveforms, including frequency-modulated continuous wave (FMCW), Doppler, and impulse radio ultra-wideband (IR-UWB) radars. First, FMCW radar is primarily considered in autonomous driving systems due to its capability to estimate range, angle, and velocity [5]. However, its use as an incabin radar may lead to potential interference issues. Second, while Doppler radar is specialized for motion detection, it is not suitable for seat occupancy monitoring since it cannot provide range information [6]. On the other hand, IR-UWB radar provides high range resolution and can be implemented with low power and cost [7], making it advantageous for incabin seat occupancy monitoring scenarios.

There have been several studies on seat occupancy monitoring using radars [8], [9]. First, in [8], an FMCW radar

was mounted on the rearview mirror to cover the entire incabin space. However, since the rearview mirror is positioned at the center of the vehicle and IR-UWB radar specializes in range estimation, this configuration cannot distinguish between seats located at symmetric positions, thereby necessitating the deployment of additional radars. In [9], two IR-UWB radars were deployed to detect occupancy of four seats in a five-seat vehicle. However, the driver's seat was not taken into account, and if five seats, including the driver's seat, were to be identified, using only two radars would not be sufficient to achieve high classification accuracy.

Therefore, this paper proposes an algorithm for in-cabin seat occupancy monitoring using multiple IR-UWB radars, which utilizes a respiration rate-based method to identify human targets. This approach enables distinguishing human targets from non-human objects that may cause false alarms. Furthermore, seven different radar positions are evaluated, and various combinations of these radar positions are compared using the proposed algorithm to determine the optimal radar combination for achieving the desired performance.

The remainder of this paper is organized as follows. Section II explains the IR-UWB radar signal considering human targets. The proposed respiration rate-based human detection algorithm and seat positioning algorithm is described in Section III. Section IV presents the experimental setting and results, and Section V concludes this paper.

II. IR-UWB RADAR SIGNAL ANALYSIS

A. Basic IR-UWB radar signal

IR-UWB radar signals are generated using pulse-shaped baseband signals characterized by a wide frequency bandwidth and short duration. Since available frequency bands are regulated differently by country, these baseband signals are modulated to operate within the frequency bands allocated for each region.

$$s(t) = p(t)\cos(2\pi f_c t),\tag{1}$$

where p(t) is the pulse waveform and f_c is the carrier frequency. Among the various pulse waveforms available, gaussian pulses are the most widely used. The Gaussian pulse is related to the $-10~\mathrm{dB}$ bandwidth of the radar, f_B , as follows:

$$p(t) = A \exp\left(\frac{-t^2}{2\tau^2}\right), \quad \tau = \frac{1}{\pi f_B \sqrt{\log_{10} e}}, \quad (2)$$

where A is the amplitude and τ represents the pulse duration parameter.

When a transmitted signal propagates forward, is reflected by an object, and is subsequently received by the radar module, the module analyzes its characteristics to extract information about the object. The signal received at the n-th observation can be expressed as follows:

$$r_n(t) = \sum_{k=1}^K \alpha_k s(t - \tau_k) + w(t), \tag{3}$$

where α_k and τ_k are the attenuated amplitude and time delay by the k-th path, K is the number of paths and w(t) is additive noise, respectively. After digitization through an analog-to-digital converter (ADC) for signal processing, it can be expressed as a row vector.

$$\mathbf{r}_{n} = [r_{n}[1], r_{n}[2], \cdots, r_{n}[M]],$$

$$r_{n}[m] = r_{n}(mT_{s}) \quad (m = 1, 2, \cdots, M),$$
(4)

where m denotes the sample index, T_s is the sampling period. And M denotes the number of samples, which is determined by the reception time and the sampling frequency of the radar module. Because the target-reflected signal is delayed by the round-trip time between the radar and the target, the m-axis can be interpreted as the distance axis. Furthermore, when N radar received signals are stacked to form an N-by-M matrix, the rows correspond to fast-time samples (distance axis), while the columns correspond to the slow-time samples (time axis). Accordingly, in this paper, the row direction is referred to as the fast-time or distance axis, and the column direction is referred to as the slow-time or simply the time axis.

B. Reflected signals from humans

Based on the assumption that human breathing is periodic [10], the distance formula between the radar and the human can be expressed as follows:

$$d_{human}(t) = d_0 + \Delta d(t) = d_0 + A_r \cos(2\pi f_r t) + A_h \cos(2\pi f_h t),$$
 (5)

where d_0 denotes the distance between the radar and the human, $\Delta d(t)$ denotes the micro-displacement due to respiration and heartbeat, A_r and A_h denote the amplitude of respiration (4–12 mm) and heartbeat (0.1–0.5 mm), and f_r and f_h denote their respective frequencies, respiration (0.1– 0.5 Hz) and heartbeat (0.8-2.0 Hz). The amplitude of the heartbeat is considerably smaller than that of respiration. Consequently, heartbeat detection requires identifying extremely subtle movements, which becomes challenging when such signals are masked by other motions. For this reason, the present study focuses on observations associated with respiratory activity. If a human remains stationary, d_0 remains constant while only $\Delta d(t)$ varies. These microscopic displacements around d_0 cause the intensity of the received signal at that point to periodically fluctuate with the same period. By collecting received signals over time and arranging each row vector into a matrix, it can be observed that the intensity of the signal in the column corresponding to the human's location periodically varies.



Fig. 1: X4M03 IR-UWB radar

III. PROPOSED RESPIRATION RATE-BASED ALGORITHM

The human detection and seat positioning techniques proposed in this paper are described in the follows. First, each radar detects the human's respiration rate and estimates the distance from that radar to the human based on the nearest point at which the respiration signal is observed. Then, by using radars that detect an identical respiration rate, the human's seat position is estimated.

A. Preprocessing

First, to extract the radar signal within the desired band, each received signal of length M is passed through a band-pass filter matched to the center frequency and bandwidth. A total of N received signal vectors are collected over the reception time to construct the radar signal signal matrix. Next, clutter removal is performed using the mean subtraction technique, which mitigates reflections from unwanted stationary objects by subtracting the mean values across the columns of the radar signal matrix [11].

B. Respiration rate-based in-vehicle human detection

To estimate the human respiration rate of a radar, a Fast Fourier Transform(FFT) is applied along the column direction of the radar signal matrix, i.e., the slow-time axis. From the resulting matrix after applying the slow-time FFT, two frequency-domain features are proposed for detecting human presence and estimating the respiration rate. The first feature, f_{LMI} , is the Local Maximum Indicator (LMI), which represents the number of distance samples at a given frequency where the frequency component is a local maximum relative to its neighboring frequencies. The second feature, f_{MP} , is the Maximum Peak (MP), which represents the maximum value at each frequency in the slow-time FFT-processed radar signal matrix. The two frequency features are defined as follows:

$$f_{LMI}[f] = \frac{1}{\bar{M}} \Sigma_{\bar{m} \in \bar{M}} \mathbf{1}_{local_{max}} (R_{FFT}[f, \bar{m}]), \qquad (6)$$

$$f_{MP}[f] = \max(R_{FFT}[f, \bar{m}]), \tag{7}$$

where f denotes the frequency sample index within the frequency band of respiration rate, \bar{m} denotes the distance sample index within the detection range, and \bar{M} is the number of distance samples in the detection range, $R_{FFT}[f,m]$ represents the radar signal matrix after slow-time FFT, and $\mathbf{1}_{localmax}(R_{FFT}[f,\bar{m}])$ is an indicator function that returns

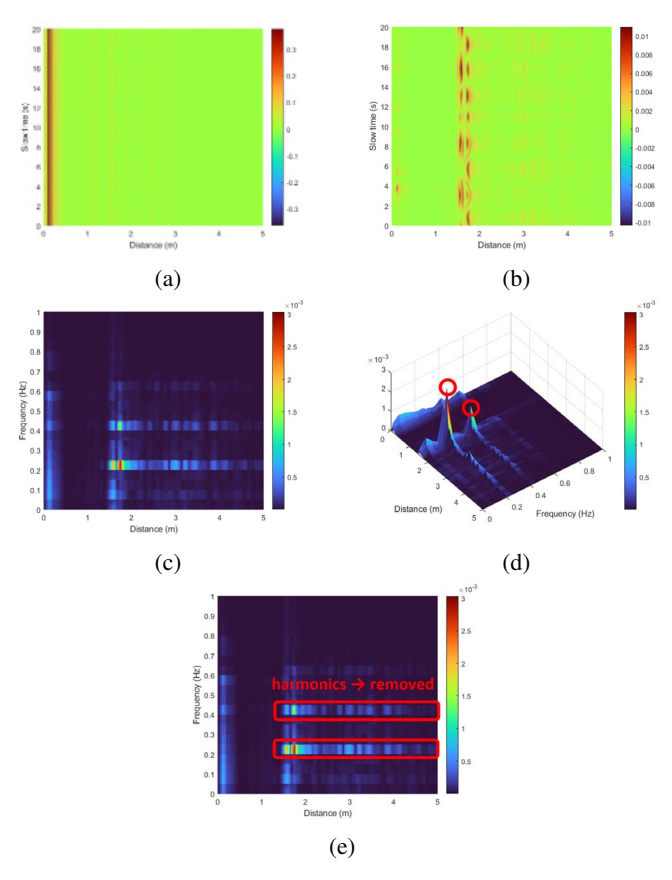


Fig. 2: Human at 1.5 m with 0.2 respiration rate (a) Raw radar data (b) Radar signal after clutter removal (c) Radar signal after FFT on the slow-time axis (d) Respiration rate estimation using frequency characteristics (e) Harmonics removal

1 if $R_{FFT}[f,\bar{m}]>R_{FFT}[f-1,\bar{m}]$ and $R_{FFT}[f,\bar{m}]>R_{FFT}[f+1,\bar{m}]$ and 0 otherwise.

After obtaining the frequencies at which the product of the two feature values exceeds the predefined threshold δ_{th} , the frequency components corresponding to integer multiples of the fundamental frequency are removed to suppress harmonics and create a human respiration rate set of l-th radar, F_l .

$$F_l = \{ f^* | f_{LMI}[f^*] \times f_{MP}[f^*] > \delta_{th} \}. \tag{8}$$

Additionally, the distance between the person and l-th radar's corresponding to the estimated respiration rate is identified as the shortest distance at which the product of the two frequency features exceeds the threshold. The set of distance samples corresponding to the respiration rate estimated by the l-th radar, denoted as M_l , is defined as

$$M_{l} = \{ \bar{m}(f^{*}) | \min_{\bar{m}} (f_{LMI}[f^{*}] \times R_{FFT}[f^{*}, \bar{m}] > \delta_{th})$$
 for $f^{*} \in F_{l} \}$, (9)

Then, when using multiple radars in combination, specify the minimum number of radars, N_{min} required for detection. If the same respiration rate is detected by more than the specified

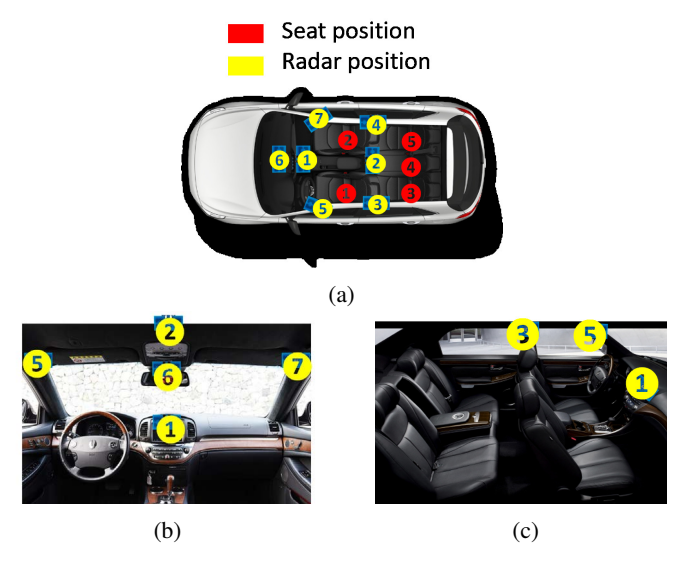


Fig. 3: Experiment Environment

minimum number of radars, the vehicle is determined to have a person with that respiration rate. Then, the set of finally detected respiration rates is defined as follows:

$$F^{N_{min}} = \{ f | \Sigma_{l=1}^{L} \mathbf{1}_{f \in F_{l}} \ge N_{min} \}.$$
 (10)

C. Seat positioning

Through the above process, each radar estimates the human's respiration rates and distances. The seat position is estimated using radars that measure the same respiration rate. Here, a predefined dictionary is used which is composed of reference distances from each radar to each seat position. The seat position that minimizes the 1-norms of the error between the estimated distances and reference distances is determined as follows:

$$\tilde{p}_r = \min_{p} \sum_{q \in Q(f_r^{N_{min}})} |D(p, q) - \tilde{d}_{qr}|, \tag{11}$$

where \tilde{p}_r denotes the estimated seat position of the $f_r^{N_{min}}$ which is the r-th member of the set $F^{N_{min}}$. $Q(f_r^{N_{min}}) = \{l|f_r^{N_{min}} \in F_l \text{ for } f_r^{N_{min}} \in F^{N_{min}}\}$ represents the set of radars that detected a respiration rate $f_r^{N_{min}}$. D(p,q) denotes a distance dictionary representing the distance from the p-th seat to the q-th radar as a p by q matrix. And \tilde{d}_{qr} denotes the distance at which the $f_r^{N_{min}}$ is detected by the q-th radar.

IV. EXPERIMENTS AND RESULTS

The experiment was conducted using Xethru's X4M03 module (Fig. 1). The specifications of the radar and the parameters configured for the experiment are summarized in the Table I. A typical five-seater passenger vehicle was selected as the experimental environment, and seven radars were installed at different locations. As illustrated in the figure, each radar location is denoted by a number in a yellow circular marker, while each seat position is indicated by a number in a red circular marker (Fig. 3). The locations of radars 1 through 7

are the center fascia, the center of the ceiling, the top of the left and right B-pillars, the top of the left A-pillar, the rear-view mirror, and the top of the right B-pillar, respectively. Radars 3 and 4 were primarily installed to monitor the rear seats.

TABLE I: X4M03 IR-UWB radar specification

Parameter	
Center frequency	7.29 GHz
Bandwidth	1.4 GHz
Transmission power	4.1 dBm
Frame duration	5 m
Sampling frequency	23.328 GHz
Measured time	60 sec
Frames per second	100

Data were collected under various scenarios involving one object (O) and two persons (P1, P2) (Table II). To evaluate the false alarm performance, an object with a large volume was employed. For each scenario, radar signals were recorded for 60 seconds and segmented using a 5-second shift to generate 20-second radar signal matrices for analysis. To identify the optimal number and placement of radar sensors for detecting and localizing occupants inside a vehicle, multiple radar combinations were evaluated. Two performance metrics were defined: Detection Accuracy, representing the ability to identify the presence of a person, and Positioning Accuracy, indicating the accuracy of seat-level localization. The scenarios summarized in Table II are classified as follows. Scenarios 1–10 correspond to cases involving only objects or only individuals. Scenarios 11-26 correspond to cases in which one individual coexists with one object. Scenarios 27-36 correspond to cases involving two individuals. Finally, Scenarios 37-60 correspond to cases in which two individuals coexist with one object.

The detection and positioning accuracies for all radar combinations were computed, and the optimal performance with respect to the number of radars employed is presented in Fig. 4. The results for Scenarios 1–26, which include at most one individual, are depicted by the blue line, whereas the results for Scenarios 1–60, which include up to two individuals, are depicted by the red line. In all cases, the detection accuracy exceeded 99%. In scenarios involving at most one individual, the positioning accuracy reached 98.56% when four or five radars were employed, specifically with the radar combinations [4, 5, 6, 7] and [3, 4, 5, 6, 7]. Across all scenarios, the highest positioning accuracy, 71.04%, was achieved with three radars, using the combination [5, 6, 7]. These results indicate that the best performance was obtained when employing three or four radars, whereas the use of additional radars led to performance degradation. Radar 2, installed on the ceiling, demonstrated comparatively lower detection performance, indicating that its inclusion in a radar combination may lead to a reduction in overall system performance.

V. CONCLUSION

This paper proposes an algorithm for detecting the presence of a human inside a vehicle and estimating their seat

TABLE II: Scenarios

Scenarios	Seat 1	Seat 2	Seat 3	Seat 4	Seat 5
1	X	X	X	X	X
2	X	О	X	X	X
3	X	X	0	X	X
4	X	X	X	0	X
5	X	X	X	X	0
6	P1	X	X	X	X
7	X	P1	X	X	X
8	X	X	P1	X	X
9	X	X	X	P1	X
10	X	X	X	X	P1
11	P1	0	X	X	X
12	X	0	P1	X	X
13	X	0	X	P1	X
14	X	0	X	X	P1
15	P1	X	0	X	X
16	X	P1	0	X	X
17	X	X	0	P1	X
18	X	X	0	X	P1
19	P1	X	X	0	X
20	X	P1	X	0	X
21	X	X	P1	0	X
22	X	X	X	0	P1
					0
23	P1	X	X	X	-
24	X	P1	X	X	0
25	X	X	P1	X	0
26	X	X	X	P1	0
27	P1	P2	X	X	X
28	P1	X	P2	X	X
29	P1	X	X	P2	X
30	P1	X	X	X	P2
31	X	P1	P2	X	X
32	X	P1	X	P2	X
33	X	P1	X	X	P2
34	X	X	P1	P2	X
35	X	X	P1	X	P2
36	X	X	X	P1	P2
37	P1	O	P2	X	X
38	P1	О	X	P2	X
39	P1	O	X	X	P2
40	X	О	P1	P2	X
41	X	О	P1	X	P2
42	X	0	X	P1	P2
43	P1	P2	0	X	X
44	P1	X	0	P2	X
45	P1	X	О	X	P2
46	X	P1	0	P2	X
47	X	P1	О	X	P2
48	X	X	0	P1	P2
49	P1	P2	X	0	X
50	P1	X	P2	0	X
51	P1	X	X	0	P2
52	X	P1	P2	0	X
53	X	P1	X	0	P2
54	X	X	P1	0	P2
55	P1	P2	X	X	0
56	P1	X	P2	X	0
57	P1	X	X	P2	0
58	X	P1	P2	X	0
59	X	P1	X	P2	0
60	X	X	P1	P2	0
00	Λ	Λ	11	1 4	U

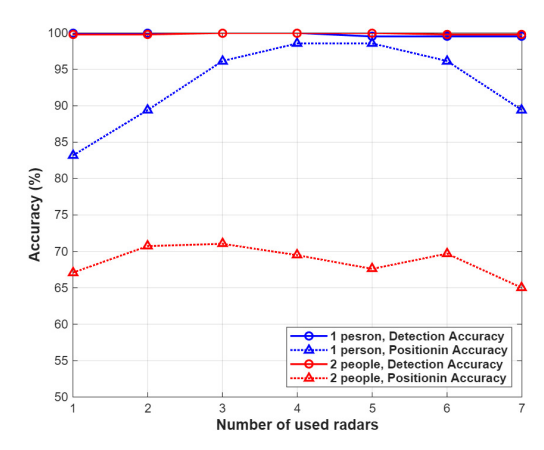


Fig. 4: Results of the experiments

position using impulse radio ultra-wideband (IR-UWB) radar. When multiple radars are deployed, the algorithm utilizes the consistency of respiration rates to associate signals measured independently by each radar as originating from the same person. Using this algorithm, a human detection accuracy exceeding 99% was achieved.

By evaluating various radar placements with the proposed algorithm, optimal configurations were identified, achieving over 70% accuracy in scenarios with large objects and up to two individuals, and over 98% accuracy in single-individual scenarios.

ACKNOWLEDGMENT

This work was supported by the Technology Innovation Program (or Industrial Strategic Technology Development Program, No. 20014098, Development of 4D Imaging Radar Sensor Module for Autonomous Driving) funded by the Ministry of Trade, Industry & Energy (MOTIE, Korea).

REFERENCES

- X. Zeng, F. Wang, B. Wang, C. Wu, K. J. R. Liu, and O. C. Au, "In-vehicle sensing for smart cars," *IEEE Open Journal of Vehicular Technology*, vol. 3, pp. 221–242, 2022.
- [2] J. Wang, W. Chai, A. Venkatachalapathy, K. L. Tan, A. Haghighat, S. Velipasalar, Y. Adu-Gyamfi, and A. Sharma, "A survey on driver behavior analysis from in-vehicle cameras," *IEEE Transactions on Intelligent Transportation Systems*, vol. 23, no. 8, pp. 10186–10209, 2021.
- [3] J. G. Valero, G. González-López, A. A. Expósito, L. V. Estrada, and F. J. Lobo, "Automotive in-cabin radar uncovered: The essential guide to choose the perfect sensing technology for your vehicle," *IEEE Transactions on Microwave Theory and Techniques*, 2025.
- [4] A. Gharamohammadi, A. Khajepour, and G. Shaker, "In-vehicle monitoring by radar: A review," *IEEE Sensors Journal*, vol. 23, no. 21, pp. 25650–25672, 2023.
- [5] M. Jankiraman, FMCW radar design. Artech House, 2018.
- [6] C. Li, V. M. Lubecke, O. Boric-Lubecke, and J. Lin, "A review on recent advances in doppler radar sensors for noncontact healthcare monitoring," *IEEE Transactions on microwave theory and techniques*, vol. 61, no. 5, pp. 2046–2060, 2013.
- [7] M. Cheraghinia, A. Shahid, S. Luchie, G.-J. Gordebeke, O. Caytan, J. Fontaine, B. Van Herbruggen, S. Lemey, and E. De Poorter, "A comprehensive overview on uwb radar: Applications, standards, signal processing techniques, datasets, radio chips, trends and future research directions," *IEEE Communications Surveys & Tutorials*, 2024.

- [8] S. Lim, S. Lee, J. Jung, and S.-C. Kim, "Detection and localization of people inside vehicle using impulse radio ultra-wideband radar sensor," *IEEE Sensors Journal*, vol. 20, no. 7, pp. 3892–3901, 2019.
- [9] S.-Y. Kwon and S. Lee, "In-vehicle seat occupancy detection using ultrawideband radar sensors," in 2022 23rd International Radar Symposium (IRS), pp. 275–278, IEEE, 2022.
- [10] S. Venkatesh, C. R. Anderson, N. V. Rivera, and R. M. Buehrer, "Implementation and analysis of respiration-rate estimation using impulse-based uwb," in *MILCOM 2005-2005 IEEE Military Communications Conference*, pp. 3314–3320, IEEE, 2005.
- [11] A. Nezirovic, "Stationary clutter- and linear-trend suppression in impulse-radar-based respiratory motion detection," in 2011 IEEE International Conference on Ultra-Wideband (ICUWB), pp. 331–335, 2011.